

# Multiple-mode phase matching in a single-crystal lithium niobate waveguide for three-wave mixing

Chuanyi Zhu (朱传义), Yuping Chen (陈玉萍)\*, Guangzhen Li (李广珍),  
Licheng Ge (葛励成), Bing Zhu (朱兵), Mengning Hu (胡梦宁),  
and Xianfeng Chen (陈险峰)

State Key Laboratory of Advanced Optical Communication Systems and Networks, School of Physics and Astronomy, Shanghai Jiao Tong University, Shanghai 200240, China

\*Corresponding author: ypchen@sjtu.edu.cn

Received March 28, 2017; accepted May 23, 2017; posted online June 15, 2017

Developing natural “free space” frequency upconversion is essential for photonic integrated circuits. In a single-crystal lithium niobate thin film planar waveguide of less than 1  $\mu\text{m}$  thickness, we achieve type I and type II mode phase-matching conditions simultaneously for this thin film planar waveguide. Finally, by employing the mode phase matching of  $e + e \rightarrow e$  with  $d_{33}$  at 1018 nm, we successfully achieve a green second-harmonic wave output with the conversion efficiency of  $0.12\%/(W \cdot \text{cm}^2)$ , which verifies one of our simulation results. The rich mode phase matching for three-wave mixing in a thin film planar waveguide may provide a potential application in on-chip frequency upconversions for integrated photonic and quantum devices.

OCIS codes: 190.4390, 130.3730, 190.2620.

doi: 10.3788/COL201715.091901.

Lithium niobate (LN) is attractive for investigations due to its intriguing electro-optical, acousto-optical and optical nonlinear properties<sup>[1,2]</sup>. In addition, LN crystal has an optical transparency window with a large bandwidth from 350 to 5200 nm, which offers a wide range of phase-matching possibilities<sup>[3–6]</sup>. Furthermore, single-crystal LN thin film has attracted intensive research interest because of the rapid commercial development of chip-scale fabrication techniques<sup>[7,8]</sup>. Recently, a vast number of integrated optical components based on single-crystal LN thin film, such as waveguides<sup>[9]</sup>, whispering gallery mode cavities have been successfully designed and fabricated<sup>[10–12]</sup>.

Due to the expensive and time-consuming fabrication of LN chip-scale devices<sup>[13,14]</sup>, the theoretical simulations and predictions become really important, especially for researchers. Based on LN thin film, there are some works on second-harmonic generation (SHG) in strip waveguides<sup>[15–17]</sup>. In this Letter, we tried to study the intrinsic quadratic phase-matching conditions in the single-crystal LN thin film as a natural planar waveguide structure. We predicted different mode phase-matching conditions for three-wave mixing in single-crystal LN thin films of different thicknesses by theoretical simulation and then at 1018 nm pump light we observed a green SHG light of 509 nm with the highest nonlinear coefficient  $d_{33}$ <sup>[18,19]</sup>, corresponding to one of the mode phase-matching points. By analyzing and calculating the dispersion relations of waveguides in LN thin films with different thicknesses, we found that for the guiding wave confined in the film, the larger the thickness is, the larger the mode size and effective refractive index are. Specifically, we gave full possibilities of types I and II mode phase-matching of SHG in a 900 nm single-crystal LN thin film planar waveguide, where type I phase matching of SHG includes

$e + e \rightarrow e$ ,  $o + o \rightarrow e$ ,  $o + o \rightarrow o$  and type II SHG includes  $e + o \rightarrow o$  and  $e + o \rightarrow e$ . The spontaneous parametric downconversion (SPDC) was also analyzed by studying type II SHG at 1.55  $\mu\text{m}$  for the  $e + o \rightarrow o$  case.

During the three-wave mixing in LN, the energy and momentum conservation must be satisfied<sup>[19–21]</sup>. They can be expressed by

$$\omega_1 + \omega_2 = \omega_3, \quad (1)$$

$$\Delta \vec{k} = \vec{k}_3 - (\vec{k}_1 + \vec{k}_2), \quad (2)$$

where  $k_i = n_i \omega_i / c$  ( $i = 1, 2, 3$ ),  $\omega_i$  and  $\vec{k}_i$  represent the frequency and wave vector, respectively. When  $\vec{k}_1$  and  $\vec{k}_2$  are equal, the three-wave mixing represents the SHG. The second-harmonic (SH) waves can be efficiently generated after satisfying the phase-matching condition  $\Delta \vec{k} = 0$ , in which the refractive indices of the fundamental wave (FW)  $n_1$  and SH wave  $n_3$  must be the same. Generally, the condition of  $n_1 = n_3$  cannot be satisfied because of the intrinsic material dispersion.

A schematic diagram of LN on insulator (LNOI) is shown in Fig. 1(a); 1.9  $\mu\text{m}$  silica is sandwiched by LN thin film and the LN substrate<sup>[22]</sup>. Figure 1(b) illustrates the propagation path of guiding mode waves.  $n_f$ ,  $n_c$ , and  $n_s$  represent the refractive indices of the thin film layer (guiding layer), air (cladding layer), and silica layer (substrate layer), respectively.  $h$  is the thickness of the guiding layer, which can be processed ranging from 300 to 900 nm. Figure 1(c) is the two different mode field distributions in the film with the thicknesses of 300 and 900 nm, respectively. The mode field distribution under different thicknesses has different areas, which is shown in Fig. 1(d). It represents the relationship between the mode size and the

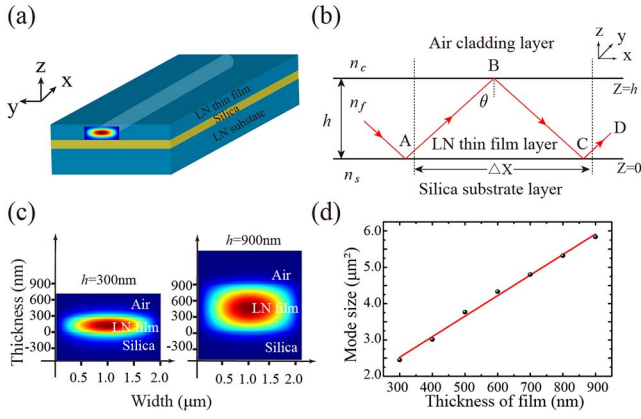


Fig. 1. (a) Schematic diagram of LN thin film. The blue light line represents the light beam at 1018 nm propagating in the planar waveguide. (b) A sectional view of the waveguide and propagation of guiding mode waves. (c) Mode field distributions when the thicknesses of the film are 300 and 900 nm, respectively. (d) The mode size versus different thicknesses of the film.

thickness of the film, which is approximately linear. For the guiding wave confined in the film, the larger the thickness is, the smaller the mode field mismatch is, and the higher the coupling efficiency is. It is worth noting that we use  $Z$ -cut 5% MgO-doped LN thin film at 25°C.  $n_f$  of LN satisfies the Sellmeier equation<sup>[23,24]</sup>, and  $n_s$  of silica is uniformly set as 1.45. Assuming that the wave propagates along path ABCD in Fig. 1(b), the total horizontal ( $Z$  axis direction) phase shift is:

$$2k_0 n_f \cos \theta \cdot h + \varphi_{fc} + \varphi_{fs}. \quad (3)$$

Here,  $k_0$  represents the wave vector in a vacuum,  $\theta$  represents the reflection angle, and  $\varphi_{fc}$  and  $\varphi_{fs}$  represent the total reflection phase shift of point B and point C, respectively. It should be noticed that the TE- and TM-polarized definitions of  $\varphi_{fc}$  and  $\varphi_{fs}$  are different. They are given by

$$\tan \frac{\varphi_{fc}}{2} = \begin{cases} -\frac{\sqrt{n_f^2 \sin^2 \theta - n_c^2}}{n_f \cos \theta} & \text{TE-polarized,} \\ -\frac{n_f \sqrt{n_f^2 \sin^2 \theta - n_c^2}}{n_c^2 \cos \theta} & \text{TM-polarized.} \end{cases} \quad (4)$$

$$\tan \frac{\varphi_{fs}}{2} = \begin{cases} -\frac{\sqrt{n_f^2 \sin^2 \theta - n_s^2}}{n_f \cos \theta} & \text{TE-polarized,} \\ -\frac{n_f \sqrt{n_f^2 \sin^2 \theta - n_s^2}}{n_s^2 \cos \theta} & \text{TM-polarized.} \end{cases} \quad (5)$$

Generally, when light propagates along the  $X$  axis in a  $Z$ -cut LN thin film, TE and TM guiding modes represent the ordinary (o) and extraordinary (e) waves, respectively.

In order to form a guiding mode in the guiding layer, Eq. (3) has to satisfy the eigenvalue equation<sup>[25]</sup>

$$2k_0 n_f \cos \theta \cdot h + \varphi_{fc} + \varphi_{fs} = 2m\pi, \quad (6)$$

where  $m$  ( $m = 0, 1, 2, \dots$ ) is the mode number. A finite number of  $m$  means the reflection angle is also limited. The effective refractive index  $n_{\text{eff}}$  ( $n_{\text{eff}} = n_f \sin \theta$ ) represents different modes for a specific waveguide structure. Incident angles of the FW that can be constrained in the waveguide are also discrete. That means that different modes correspond to different  $\theta$ .  $n_{\text{eff}}$  is determined by  $n_f$ ,  $\theta$ , and  $m$  for a specific waveguide structure (fixed values of  $n_c$ ,  $n_s$ , and  $h$ ) from Eq. (6). A searching method called stepwise extension is used to solve the eigenvalue equation and to obtain the effective refractive index of the planar waveguide. In order to generate an SH wave, we chose an LN thin film planar waveguide as a specific structure corresponding to different wavelengths that could satisfy the phase-matching condition  $n_{\text{eff\_FW}} = n_{\text{eff\_SH}}$  ( $n_{\text{eff\_FW}}$  and  $n_{\text{eff\_SH}}$  stand for the effective refractive indices of the FW and SH, respectively).

First, we analyzed the relationship between the wavelength  $\lambda$  and the effective refractive index  $n_{\text{eff}}$  for specific thicknesses of the layer  $h$  and polarizations. Figures 2(a) and 2(b) represent a dispersion relation of zero-order TE and TM mode which are constrained in a thin film waveguide with different thicknesses for FW and SH waves, respectively. It shows that  $n_{\text{eff}}$  has a linear decrease trend with increasing  $\lambda$ , and  $n_{\text{eff}}$  of the TE-polarized wave is larger than for the TM-polarized wave for both FW and SH waves. We also found that the larger thickness, the larger  $n_{\text{eff}}$ .

Then, we analyzed two types of SHG that both meet the phase-matching conditions. Type I means two incoming waves of the FW have the same polarizations, which includes four cases:  $e + e \rightarrow e$ ,  $e + e \rightarrow o$ ,  $o + o \rightarrow e$ , and  $o + o \rightarrow o$ . Type II means their polarizations are orthogonal with respect to each other, which includes types  $e + o \rightarrow o$  and  $e + o \rightarrow e$ .

In Fig. 3, we presented three type I mode phase matchings for 900 nm thin film. Here, in definition, the case of  $o + o \rightarrow o$  means that both FW and SH waves are TE-polarized. The phase matching of  $e + e \rightarrow o$  is invalid because in LN (point group 3m) there is no corresponding nonlinear tensor element<sup>[19]</sup>. The lines in different colors represent the effective indices  $n_{\text{eff}}$  of different modes, where solid and dashed lines represent FW and SH waves,

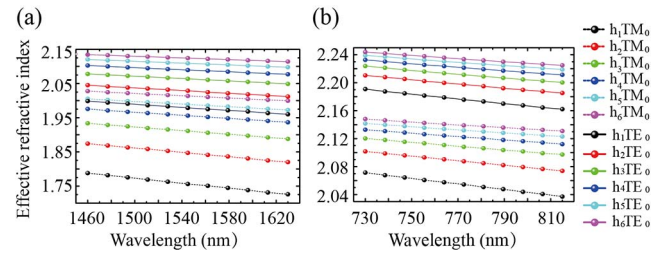


Fig. 2. (Color online) Dispersion relation of TE- and TM-polarized modes for (a) FW and (b) SH waves in LN thin film with different thicknesses at 25°C.  $h_1, h_2, h_3, h_4, h_5$ , and  $h_6$  represent thicknesses of the layers, which are 500, 600, 700, 800, 900, and 1000 nm, respectively.

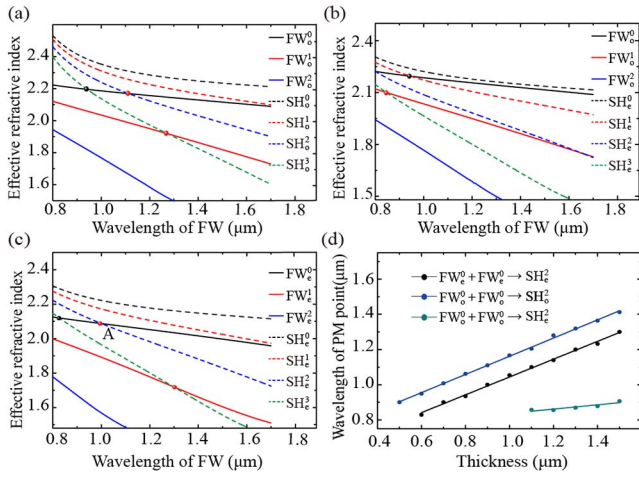


Fig. 3. (Color online) Three-mode phase-matching diagrams in 900 nm LN thin film: (a)  $o + o \rightarrow o$ ; (b)  $o + o \rightarrow e$ ; (c)  $e + e \rightarrow e$ . The solid and dashed lines represent FW and SH waves, respectively, and the black, red, blue, and green lines represent the 0th, 1st, 2nd, and 3rd orders of the space guiding modes. The black points on the intersection stand for nonoverlapping of the space-mode field distribution for the FW and SH waves. The red points stand for the simultaneous satisfaction of the space-mode overlapping and phase-matching modes of the FW and SH waves. (d) The wavelength of the phase-matching point between the 0th FW and 2nd SH waves varies almost linearly with the thickness of the thin film.

respectively. The intersections between different lines are phase-matching points. We found that the overlap integrals of the interaction waves were 0.0681 for the 0th to 2nd modes and only 0.0020 for the 0th to 1st modes<sup>[26]</sup>. Taking those into consideration, some phase-matching conditions cannot be used to achieve the effective SHG because of the poor overlap of the space-mode field distributions with each other, such as the overlap between odd and even mode fields. We marked the bad overlap with black points. On the contrary, the red points have a good overlap where the SH wave can be generated efficiently. In Fig. 3(c), point A satisfies the phase matching and space-mode fields matching simultaneously, where SHG could exist near 1018 nm in the 900 nm thickness of the LN thin film. Then we show this SHG experiment around 1018 nm in the experimental part, since it utilizes the largest nonlinear coefficient  $d_{33}$ .

In Fig. 3(d), we draw the whole natural phase-matching “map,” which represents the relationship between the phase-matching wavelength and the thickness of the thin film. As shown in Fig. 3(d), the wavelength of the phase-matching point increases with the increase of thickness in three effective type I phase-matching situations:  $e + e \rightarrow e$ ,  $o + o \rightarrow o$ , and  $o + o \rightarrow e$ .

The type II SHG shown in Fig. 4(a) means that the FW of 1.55  $\mu\text{m}$  has the orthogonal polarizations, and includes the two possible phase-matching cases:  $e + o \rightarrow o$  and  $e + o \rightarrow e$ . We just checked one case of  $e + o \rightarrow o$ . When the FW of 1.55  $\mu\text{m}$  with both the TM- and TE-polarized is

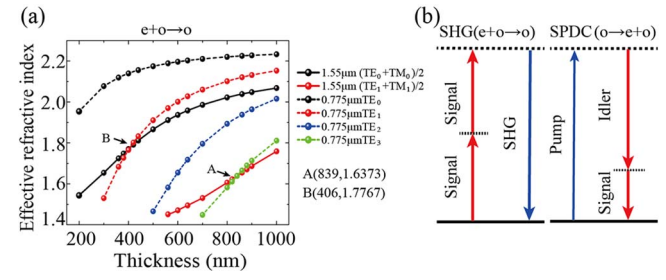


Fig. 4. (Color online) (a) Type II mode phase matching for SHG:  $e + o \rightarrow o$ , where the FW is 1.55  $\mu\text{m}$  with both the TE- and TM-polarized modes, SH is 0.775  $\mu\text{m}$  with the TE-polarized mode. (b) A schematic of SHG ( $e + o \rightarrow o$ ) and SPDC ( $o \rightarrow e + o$ ).

incident into LN thin film (as shown in Fig. 1), SH should be TE-polarized. The black solid line stands for the FW with TM- and TE-polarized of zero-order mode fields, while black dashed line stands for TE-polarized SH wave with of the zero-order mode field.

In Fig. 4(a), the two line intersects in point A (839 nm, 1.6373), which means SH generates in the case when the thickness of LN thin film is 839 nm and the effective refractive indices of the FW and SH are both equal to 1.6373. Point A stands for the condition in which SHG could happen. Oppositely, point B cannot generate SHG efficiently due to the lack of space-mode field overlap, as we mentioned above. In particular, the phenomena of the SHG and SPDC could be inverse to each other in nonlinear optics, which is shown in Fig. 4(b). It has been proven that SPDC is one of the most effective methods of generating single-photon pairs, including polarization entanglement photon-pair sources, which plays an important role in quantum communication<sup>[27,28]</sup>.

Experimentally, we chose the predicted-mode phase-matching condition of point A in Fig. 3(c) to generate a SH wave by using the largest nonlinear coefficient  $d_{33}$ . The experimental setup is shown in Fig. 5(a). At a room temperature of 25°C, a picosecond pulse laser with 2.4 ps at 1018 nm was focused into the single-crystal 5% MgO-doped congruent LN thin film sample of 900 nm thickness (supplied by NANOLN). The first polarizer behind the laser source was used to keep the fundamental light as an extraordinary light. The first lens with a 100 mm focal length (Daheng Optics, GCL-010129) was used to focus and couple the incident beam into the LN thin film, which was placed on a five-dimensional adjustable platform. The second 20 $\times$  objective lens with NA = 0.40 (BOCIC, OMO103) was used to focus the pump and green light after the crystal into the corresponding detectors. The second polarizer was used to measure the polarization of the SH wave. A prism before the detector could separate the FW and SH waves. The detectors are placed to measure the light intensity and the spectrum.

We generated an SH wave with a wavelength of 509 nm successfully. Figure 5(b) shows the top view of the green light captured by camera. The spectra of the pump and the SH waves are shown in Fig. 5(c). The generated SH

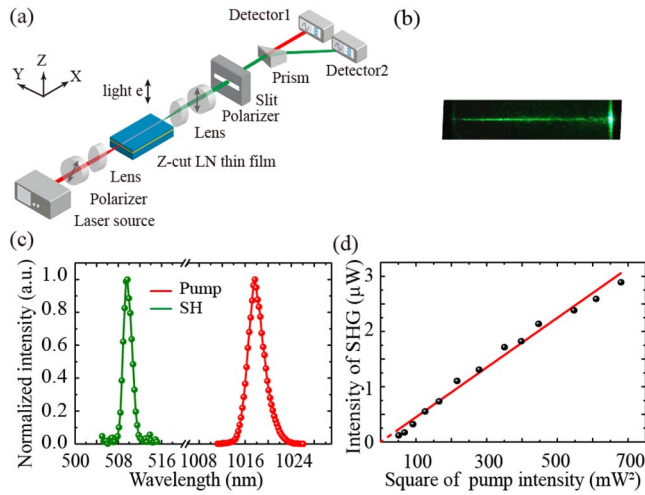


Fig. 5. (Color online) Mode phase matching SHG experiment. (a) The sketch of the experimental setup. (b) The top view of the green light field captured by the camera. (c) The spectra of the input pulse laser and the output SH light at 509 nm (for the 1018 nm pump light), respectively. (d) The quadratic intensity relationship between the TM-polarized SH and FW waves.

light in single-crystal LN film is located at 509 nm. The central wavelength of the input picosecond pulse laser is 1018 nm. It was in agreement with one of our theoretical predictions. We also verified the quadratic relationship of the light intensity between the pump and generated SH green light, as shown in Fig. 5(d). The conversion efficiency of SHG is about  $0.12\%/(W \cdot \text{cm}^2)$ <sup>[29]</sup>, which is limited by the coupling efficiency. Integrating the grating structure or using the endface-coupling method might be worthwhile methods to improve the coupling efficiency<sup>[30,31]</sup>.

In this Letter, we introduce a method of the eigenmode equation for a planar waveguide to analyze the mode phase-matching conditions. The natural types I and II phase-matching conditions are achieved by calculating the effective refractive indices with different polarization modes for single-crystal LN thin films with different thicknesses less than 1  $\mu\text{m}$ . For the SHG of incident waves with parallel polarizations, the type I phase-matching includes three cases:  $e + e \rightarrow e$ ,  $o + o \rightarrow e$ , and  $o + o \rightarrow o$ ; and we also verify the mode phase matching of  $e + e \rightarrow e$  by the SHG experiment with  $d_{33}$  at 1018 nm. As for the type II phase matching with orthogonal polarizations, we show one-mode phase matching in the case of  $e + o \rightarrow o$ . Type II nonlinear interaction may have significant applications in generating polarization-entangled photon-pair sources by SPDC when combined with a whispering-gallery-mode resonator in LN thin film. The diversified natural mode phase-matching processes in single-crystal LN thin film can find some interesting applications in on-chip photonic integrated devices.

This work was supported by the National Natural Science Foundation of China under Grant Nos. 11574208 and 61235009.

## References

1. K. K. Wong, ed., *Properties of Lithium Niobate*, EMIS Datareviews No. 28 (INSPEC, 2002).
2. M. Abarkan, M. Aillerie, N. Kokanyan, C. Teyssandier, and E. Kokanyan, *Opt. Mater. Express* **4**, 179 (2014).
3. H. Karakuzu, M. Dubov, S. Boscolo, L. A. Melnikov, and Y. A. Mazhirina, *Opt. Mater. Express* **4**, 541 (2014).
4. G.-Z. Li, Y.-P. Chen, H.-W. Jiang, and X.-F. Chen, *Photon. Res.* **3**, 168 (2015).
5. S. Kurimura, Y. Kato, M. Maruyama, Y. Usui, and H. Nakajima, *Appl. Phys. Lett.* **89**, 191123 (2006).
6. X. Chen, P. Karpinski, V. Shvedov, A. Boes, A. Mitchell, W. Krolikowski, and Y. Sheng, *Opt. Lett.* **41**, 2410 (2016).
7. G. Poberaj, H. Hu, W. Sohler, and P. Guenter, *Laser Photon. Rev.* **6**, 488 (2012).
8. G. Poberaj, M. Koechlin, F. Sulser, A. Guarino, J. Hajfler, and P. Günter, *Opt. Mater.* **31**, 1054 (2009).
9. M. F. Volk, S. Suntsov, C. E. Rüter, and D. Kip, *Opt. Express* **24**, 1386 (2016).
10. J. Lin, Y. Xu, Z. Fang, M. Wang, J. Song, N. Wang, L. Qiao, W. Fang, and Y. Cheng, *Sci. Rep.* **5**, 8072 (2015).
11. W. C. Jiang and Q. Lin, *Sci. Rep.* **6**, 36920 (2016).
12. S. Duan, Y. Chen, G. Li, C. Zhu, and X. Chen, *Chin. Opt. Lett.* **14**, 042301 (2016).
13. H. Hu, R. Ricken, and W. Sohler, *Opt. Express* **17**, 24261 (2009).
14. G. Ulliac, V. Calero, A. Ndao, F. Baida, and M.-P. Bernal, *Opt. Mater.* **53**, 1 (2016).
15. L. Cai, Y. Wang, and H. Hu, *Opt. Commun.* **387**, 405 (2017).
16. R. Geiss, S. Saravi, A. Sergeev, S. Diziain, F. Setzpfandt, F. Schrempel, R. Grange, E.-B. Kley, A. Tünnermann, and T. Pertsch, *Opt. Lett.* **40**, 2715 (2015).
17. J.-I. Kou, Q. Wang, Z.-Y. Yu, F. Xu, and Y.-Q. Lu, *Opt. Lett.* **36**, 2533 (2011).
18. R. S. Weis and T. K. Gaylord, *Appl. Phys. A* **37**, 191 (1985).
19. R. W. Boyd, *Nonlinear Optics* (Academic, 2010).
20. J. Zhang, Y. Chen, F. Lu, and X. Chen, *Opt. Express* **16**, 6957 (2008).
21. Y. Wu, B. C. Yao, Q. Y. Feng, X. L. Cao, X. Y. Zhou, Y. J. Rao, Y. Gong, W. L. Zhang, Z. G. Wang, Y. F. Chen, and K. S. Chiang, *Photon. Res.* **3**, A64 (2015).
22. H. Han, L. Cai, and H. Hu, *Opt. Mater.* **42**, 47 (2015).
23. O. Gayer, Z. Sacks, E. Galun, and A. Arie, *Appl. Phys.* **B91**, 343 (2008).
24. D. H. Jundt, *Opt. Lett.* **22**, 1553 (1997).
25. H. Nishihara, M. Haruna, and T. Suhara, *Optical Integrated Circuits* (R. Doneuey & Sons Company, 1987).
26. L. Zhang, P. J. Chandler, P. D. Townsend, Z. T. Alwahabi, S. L. Pityana, and A. J. McCaffery, *J. Appl. Phys.* **73**, 2695 (1993).
27. M. Humault, H. Takesue, O. Tadanaga, Y. Nishida, and M. Asobe, *Opt. Lett.* **35**, 1239 (2010).
28. M. Hu, Y. Chen, G. Li, and X. Chen, *Chin. Opt. Lett.* **14**, 061301 (2016).
29. K. R. Parameswaran, R. K. Route, J. R. Kurz, R. V. Roussev, M. M. Fejer, and M. Fujimura, *Opt. Lett.* **27**, 179 (2002).
30. T. Dirk, L. Frederik Van, A. Melanie, B. Wim, T. Dries Van, B. Peter, and B. Roel, *Jpn. J. Appl. Phys.* **45**, 6071 (2006).
31. G. Li, Y. Chen, H. Jiang, and X. Chen, *Opt. Lett.* **42**, 939 (2017).